Separation Science and Technology
Publication details, including instructions for authors and subscription information:
http://www.informaworld.com/smpp/title~content=t713708471

Modeling of Desalination Using Tubular Direct Contact Membrane Distillation Modules

Fawzi A. Banat[a]; Fahmi A. Abu Al-Rub[a]; Rami Jumah[a]; Mohammed Al-Shannag[a]
[a] DEPARTMENT OF CHEMICAL ENGINEERING, JORDAN UNIVERSITY OF SCIENCE AND TECHNOLOGY, IRBID, JORDAN

Online publication date: 29 July 1999

To cite this Article Banat, Fawzi A. , Al-Rub, Fahmi A. Abu , Jumah, Rami and Al-Shannag, Mohammed(1999) 'Modeling of Desalination Using Tubular Direct Contact Membrane Distillation Modules', Separation Science and Technology, 34: 11, 2191 — 2206
To link to this Article: DOI: 10.1081/SS-100100765
URL: http://dx.doi.org/10.1081/SS-100100765

SEPARATION SCIENCE AND TECHNOLOGY, **34**(11), pp. 2191–2206, 1999

Modeling of Desalination Using Tubular Direct Contact Membrane Distillation Modules

FAWZI A. BANAT,* FAHMI A. ABU AL-RUB, RAMI JUMAH, and MOHAMMED AL-SHANNAG

DEPARTMENT OF CHEMICAL ENGINEERING
JORDAN UNIVERSITY OF SCIENCE AND TECHNOLOGY
P.O. BOX 3030, IRBID, JORDAN

ABSTRACT

A fully predictive mathematical model based on first principles of heat and mass transfer as well as vapor–liquid equilibrium was developed for desalination application via tubular direct contact membrane distillation. The model took into account the temperature and the effect of concentration polarization. The model's prediction in terms of distillate flux were validated with previously published experimental data for such process parameters as saline water and cooling water flow rates and temperatures, and feed salt concentration. The model's results agreed well with previously published experimental and theoretical work.

INTRODUCTION

The demand for good quality drinking water is steadily increasing worldwide. Increasing population, especially in developing countries, and industrialization levels, together with the desire to improve standards of living, contribute to the increased demand. Although over two-thirds of the planet's surface is covered with water, 99.3% of the total water is either too salted (oceans) or inaccessible (ice caps). Because water is potable if it contains fewer than 500 parts per million of salt, much research has gone into finding efficient methods of removing salt from seawater and brackish water. For this purpose several different processes including distillation, freezing, electro-

* To whom correspondence should be addressed. E-mail: banatf@just.edu.jo

dialysis, reverse osmosis, pervaporation, and membrane distillation have been developed (1–3).

Membrane distillation is a relatively new process. Essentially the process employs hydrophobic porous membranes which are permeable to vapor but not to the liquid phase. The membrane separates a hot or warm solution from a cooler chamber which contains either a liquid or a gas. As the process is non-isothermal, the temperature difference across the membrane creates a partial pressure gradient which causes water vapor molecules to migrate through the membrane pores from the high partial pressure side where they evaporate to the low partial pressure side where they condense, that is, from the warmer to the cooler compartment as shown in Fig. 1. When used for desalination, salt water is the hot feed solution. Pure water vapor passes through the membrane pores while the salts and other nonvolatiles remain on the warm side of the membrane. The water vapor is then directly or indirectly condensed and removed as pure water. The membrane does not contribute to the separation through its selectivity but acts as a physical support at the liquid–vapor interface (4).

The advantages of membrane distillation are: production of a high purity distillate, the absence of limitations caused by osmotic pressure effects and, most important, the distillation process takes place at moderate temperatures, making it economically attractive. Also, a relatively small temperature difference between the two liquids separated by the membrane can result in relatively high fluxes. The permeate is of better quality than the product of a conventional distillation because entrainment of droplets is avoided. The major drawback of this process is membrane wetting danger.

Different types of membrane distillation processes are considered for the recovery of water vapor once it has passed through the membrane (4–11). These types are direct contact membrane distillation (DCMD), air gap membrane distillation (AGMD), vacuum membrane distillation (VMD), and sweeping gas membrane distillation.

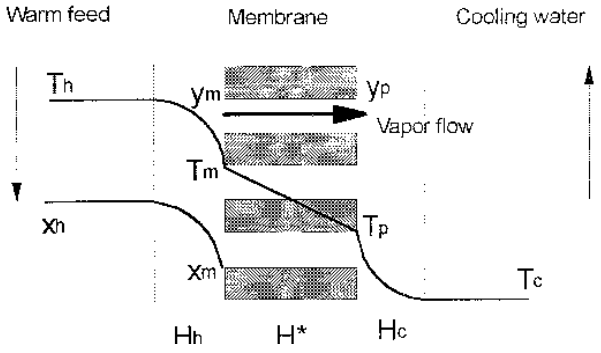

FIG. 1 Concept of the direct contact membrane distillation process.

MARCEL DEKKER, INC.
270 Madison Avenue, New York, New York 10016

The two available configurations by which membranes are packed within a module are tubular and flat sheets. The tubular configuration resembles the shell-and-tube heat exchanger except that the impermeable tubes are replaced by tubular membranes through which a radial flux takes place. In tubular configuration, both tubular and hollow fiber membranes are used. However, hollow fiber membranes provide higher surface area per unit volume, making the flux density greater than in tubular membranes. The biggest disadvantage of shell-and-tube modules is that damaged membranes cannot be replaced as easily as in flat sheet apparatuses. Therefore the module is limited by membrane life.

Flat membrane sheets were used in AGMD while in DCMD flat, tubular, and hollow fiber membranes were used. Predictive mathematical models were developed for the desalination application running AGMD in which flat sheets were used (12, 13). However, semiempirical models were presented to predict radial fluxes of desalination by DCMD in which tubular modules were used. In a series of publications, Schofield et al. (14–16) investigated the direct contact tubular configuration for the production of pure water from saline water. Their theory was based on semiempirical modeling in which the importance of temperature polarization phenomenon was emphasized. Lacoursiere (17) studied, experimentally and theoretically, the parameters that affect desalination of seawater as well as sodium chloride solutions by direct contact tubular configuration. In her mathematical model, semiempirical equations were used.

The goal of this work was to develop a fully predictive mathematical model to represent radial heat and mass transfer fluxes encountered in desalination using tubular DCMD configuration. The developed model was solely based on first principles of heat and mass transfer. Temperature and concentration polarization phenomena were considered in the model. The validity of the developed model was examined by comparing its results with Lacoursiere's published experimental results.

MATHEMATICAL MODEL

The transport of water molecules from the feed side to the condensation side, in membrane distillation, is a combined heat and mass transfer process, during which temperature and concentration gradients are established along the diffusion path. Membrane processes having a nonvolatile solute in the feed, as in desalination, exhibit a higher concentration of the solute at the evaporating surface than in the bulk. This causes a concentration polarization. In addition to that, the temperatures at the membrane interface on the feed side and on the permeate side are different from the respective bulk temperatures because of the transfer of the latent heat of vaporization to and from the mem-

brane and the sensible heat transferred across the membrane. This is referred to as temperature polarization. Knowledge of the temperatures at the interfaces is necessary in order to estimate the water flux across the membrane. These temperatures can be predicted using fundamental heat transfer principles and well-established semiempirical correlations.

Material Balances and Mass Transfer Rate Relations

According to the nomenclature shown in Fig. 2, a molar material balance along the flow path of the hot saline solution gives

$$(m_{\mathrm{f}})_{\mathrm{s}+1} = (m_{\mathrm{f}})_{\mathrm{s}} - (\overline{N}_{\mathrm{w}})_{\mathrm{s}} \tag{1}$$

where "s" refers to the segment number and $\overline{N}_{\mathrm{w}}$ is the radial molar water vapor permeation rate within that segment.

Water vapor that transports from the feed (f) is condensed in the cooling water (c) so a molar material balance along the flow path of the coolant water, after rearrangement, yields

$$(m_{\mathrm{c}})_{\mathrm{s}+1} = (m_{\mathrm{c}})_{\mathrm{s}} - (\overline{N}_{\mathrm{w}})_{\mathrm{s}} \tag{2}$$

The minus sign indicates that the coolant liquid and the feed stream are flowing countercurrently.

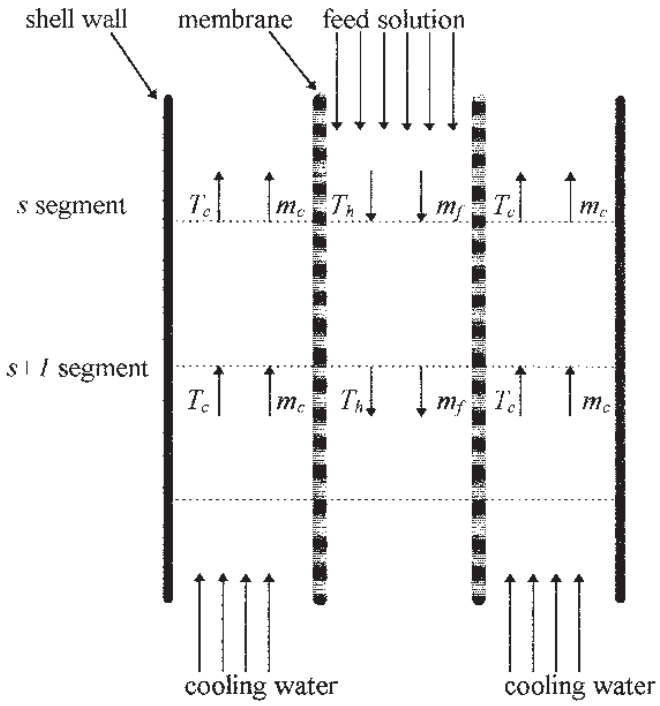

FIG. 2 Schematic diagram of the flow rate pattern.

MARCEL DEKKER, INC.
270 Madison Avenue, New York, New York 10016

In membrane distillation the hot water vapor passes through the membrane pores prior to condensation as shown in Fig. 1. Since the membrane pores are filled with air (noncondensable gas) which acts as a stagnant film, the molecular diffusion model must be applied (18). The diffusion of water vapor through a stagnant air film is known as Stefan diffusion (13). Under steady-state conditions the segmental molar flux of water vapor can be written as

$$(N)_s = \left[\frac{\overline{N}_w}{A}\right]_s = -\left[\frac{PD_{w-air}}{RT(1-y_w)}\frac{dy_w}{dr}\right]_s \tag{3}$$

where y_w is the mole fraction of water vapor, P is the total pressure [equal to the atmospheric pressure (14–17)], r is the distance in the radial direction, and A is the segment surface area open for diffusion which equals $2\varepsilon n\pi rl$, where n is the number of tubes in the module, l is the segment length, and ε is the membrane porosity which corrects for the actual open surface area for diffusion. The diffusion coefficient (D) varies with temperature according to the relation (19)

$$D_T = D_0\left(\frac{T}{T_0}\right)^{1.75} \tag{4}$$

At steady-state

$$\frac{d(\overline{N}_w)_s}{dr} = 0 \tag{5}$$

Substituting Eq. (3) into Eq. (5) and integrating over the boundary conditions:

$$\begin{aligned} &\text{at } r = r_i, \qquad y = y_m \\ &\text{at } r = r_o, \qquad y = y_p \end{aligned} \tag{6}$$

gives

$$(\overline{N}_w)_s = \varepsilon\,\frac{2\pi nlPD_{w-air}}{RT\ln\left(\frac{r_o}{r_i}\right)}\ln\left(\frac{1-y_p}{1-y_m}\right) \tag{7}$$

To correct for the actual diffusion path, the membrane thickness (δ) must be multiplied by the tortuosity factor (τ) so that $r_o = r_i + \tau\delta$.

In Eq. (7):

$$y_p = \frac{P^\circ(T_p)}{P} \tag{8}$$

$$y_m = \frac{(1-x_m)P^\circ(T_m)}{P} \tag{9}$$

where $P°(T)$ is the vapor pressure of water at that corresponding temperature, and x_m is the salt mole fraction at the membrane interface which can be obtained by simple mass balance around the nonvolatile salt:

$$(x_m)_s = \left\{ x_h \exp\left[\frac{\overline{N}_w}{n\pi d_i l \rho k_s} \right] \right\}_s \tag{10}$$

where ρ is the bulk solution molar density and k_s is the solute mass transfer coefficient. To estimate the value of k_s from Sherwood correlations, the value of NaCl–H_2O diffusivity must be known. For this purpose the Nernst–Haskell equation for dilute solutions of a single salt can be used (20). The diffusion coefficient is (20)

$$D_{NaCl–H_2O} = \frac{RT\left[\frac{1}{n^+} + \frac{1}{n^-}\right]}{F^2\left[\frac{1}{\lambda^\circ_+} + \frac{1}{\lambda^\circ_-}\right]} \tag{11}$$

To calculate the salt concentration variation along the feed flow path, it was assumed that no salt was permeating through the membrane. The conductivity measurements of the permeate flux done by Lacoursiere validate this assumption (17). Performing a salt mass balance over each segment in the direction of feed flow yields

$$(C)_{s+1} = \left[\frac{\Phi C}{\Phi - \frac{\overline{N}_w}{\rho}} \right]_s \tag{12}$$

where Φ is the volumetric flow rate of the feed solution.

Energy Balances and Heat Transfer Rate Relations

To calculate the molar water vapor transfer rate through each segment ($\overline{N}_w$), the inlet and outlet temperatures of the feed and coolant waters must be known. The hot side bulk temperature variation in the direction of feed flow can be calculated by performing an energy balance on a differential segment as shown in Fig. 2. So:

$$(T_h)_{s+1} = \frac{1}{(m_f)_{s+1}} \left[(T_h m_f)_s - \frac{(Q)_s}{C_{plw}} \right] \tag{13}$$

The heat lost from the feed solution is gained by the cooling water. Analogously, the variation of the coolant bulk temperature along the flow path is

$$(T_c)_{s+1} = \frac{1}{(m_c)_{s+1}} \left[(T_c m_c)_s - \frac{(Q)_s}{C_{plw}} \right] \tag{14}$$

The minus sign in Eq. (14) appears just because the coolant liquid and the feed stream are flowing countercurrently.

Heat transfer in membrane distillation occurs in three steps: heat flux from the feed bulk to the membrane surface, heat flux through the membrane matrix, and heat flux from the membrane outlet surface to the cooling water (see Fig. 1). The heat transfer rate $(Q)_s$ from the bulk warm feed solution toward the membrane surface can be written for each differential segment as

$$(Q)_s = \{h_{hf}A_i(T_h - T_m) + \overline{N}_w C_{plw}(T_h - T_m)\}_s = \{H_h(T_h - T_m)\}_s$$
$$(H_h)_s = \{h_{hf}A_i + \overline{N}_w C_{plw}\}_s \tag{15}$$

where h_{hf} is the liquid film heat transfer coefficient.

The heat transfer rate through the membrane matrix is given by

$$(Q)_s = [q_s + \overline{N}_w \lambda_w]_s \tag{16}$$

where q_s is the sensible heat transfer rate which includes the sensible heat carried by conduction in the normal manner without mass transfer and sensible heat carried bodily by the transferring molecules. Hence

$$(q_s)_s = \left\{-2\pi r n l k_m \frac{dT}{dr} + \overline{N}_w C_{pgw}(T - T_p)\right\}_s \tag{17}$$

where C_{pgw} is the heat capacity of water vapor and k_m is the membrane matrix thermal conductivity of the porous membrane which can be calculated from (18)

$$k_m = \varepsilon k_g + (1 - \varepsilon)k_d \tag{18}$$

where k_g and k_d are thermal conductivities of the gas phase and the solid phase, respectively. Under steady-state conditions:

$$\frac{d(q_s)_s}{dr} = 0 \tag{19}$$

Substitution of Eq. (17) into Eq. (19) and integrating with respect to the following boundary conditions

$$\text{at } r = r_i, \qquad T = T_m$$
$$\text{at } r = r_o, \qquad T = T_p \tag{20}$$

gives

$$(q_s)_s = [H^*(T_m - T_p)]_s \tag{21}$$

where

$$(H^*)_s = \left\{\overline{N}_w C_{pgw}\left[1 + \frac{1}{\left(\frac{r_i}{r_o}\right)^{-Pe} - 1}\right]\right\}_s \tag{22}$$

MARCEL DEKKER, INC.
270 Madison Avenue, New York, New York 10016

$$(\mathrm{Pe})_s = \left(\frac{\overline{N}_w C_{pgw}}{2n\pi lk}\right)_s \tag{23}$$

Substitution of Eq. (21) into Eq. (16) yields

$$(Q)_s = [H^*(T_m - T_p) + \overline{N}_w \lambda_w]_s \tag{24}$$

The heat transfer rate from the membrane surface at the permeate side to the cooling liquid bulk is

$$(Q)_s = [h_{cf} A_o (T_p - T_c) + \overline{N}_w C_{plw}(T_p - T_c)]_s = [H_c(T_p - T_m)]_s$$
$$(H_c)_s = [h_{cf} A_o + \overline{N}_w C_{plw}]_s \tag{25}$$

where h_{cf} is the liquid film heat transfer coefficient.

Solving Eqs. (15), (21), and (25) for the temperature at the membrane interface on the feed side, T_m, and the temperature at the membrane interface on the permeate side, T_p, yields

$$(T_m)_s = \left\{T_h - \frac{U_t}{H_h}\left[(T_h - T_c) + \frac{\overline{N}_w \lambda_w}{H^*}\right]\right\}_s \tag{26}$$

$$(T_p)_s = \left\{T_c + \frac{U_t}{H_c}\left[(T_h - T_c) + \frac{\overline{N}_w \lambda_w}{H^*}\right]\right\}_s \tag{27}$$

where

$$\left(\frac{1}{U_t}\right)_s = \left[\frac{1}{H_h} + \frac{1}{H^*} + \frac{1}{H_c}\right]_s \tag{28}$$

The value of the heat transfer and mass transfer coefficients can be calculated according to the hydrodynamic conditions as follows (21):

- For laminar flow:

$$\mathrm{Nu} = 1.86\left(\mathrm{RePr}\,\frac{d_h}{L}\right)^{1/3}\left(\frac{\mu_b}{\mu_m}\right)^{0.14} \tag{29}$$

$$\mathrm{Sh} = 1.86\left(\mathrm{ReSc}\,\frac{dh}{L}\right)^{1/3} \tag{30}$$

- For turbulent flow:

$$\mathrm{Nu} = 0.023\mathrm{Re}^{0.8}\mathrm{Pr}^{0.3} \tag{31}$$

$$\mathrm{Sh} = 0.023\mathrm{Re}^{0.8}\mathrm{Sc}^{0.3} \tag{32}$$

The membrane was divided into segments of differential and equal length, and the outlet feed flow rate, temperature, and concentration were calculated for each segment. Also, the temperature and salt concentration at the membrane interface were calculated for each differential segment. This required an

iterative solution of the forgoing coupled heat and mass transfer equations. The average of the inlet and outlet values was considered in calculating the permeate flux of each segment. Note that the feed solution and coolant water were flowing countercurrently; therefore, the initially guessed outlet coolant temperature and flow rate must also be solved iteratively in order to match the specified inlet conditions. A computer program was constructed to perform the calculations using suitable numerical techniques. The total flux was calculated by summing the fluxes of all segments.

RESULTS AND DISCUSSION

The model validity is examined here by comparing model predictions with Lacoursiere's published data (17) for process variables such as salinated water flow rate, cooling water flow rate, salinated water temperature, cooling water temperature, and salt concentration. The physical properties of Lacoursiere's module are presented in Table 1 (17).

Saline Water and Cooling Water Flow Rate

A comparison between model predictions and experimental data for the effect of saline water flow rate and cooling water flow rate on pure water flux is presented in Figs. 3 and 4, respectively. Here, the agreement between experimental values and the model is very good. As shown in Fig. 3, the state of distillate production is dependent on the saline water flow rate. It increases sharply at lower flow rate levels and reaches an asymptote at higher flow rates. This can be attributed to the reduction of temperature and concentration polarization at the membrane boundary and to the fact that at lower feed flow rates the hot saline solution cools down faster, and thus the vapor pressure dif-

TABLE 1
Properties of Lacoursiere's Module (17)

Membrane material	Polypropylene
Housing material	Polypropylene
Potting material	Polypropylene
Inside diameter of the shell (mm)	25
Number of tubes	3
Module length (m)	0.7
Thickness of membrane (mm)	1.5
Nominal pore diameter (μm)	0.2
Tortuosity factor	2
Effective filtration area (m^2)	0.036
Porosity	0.75

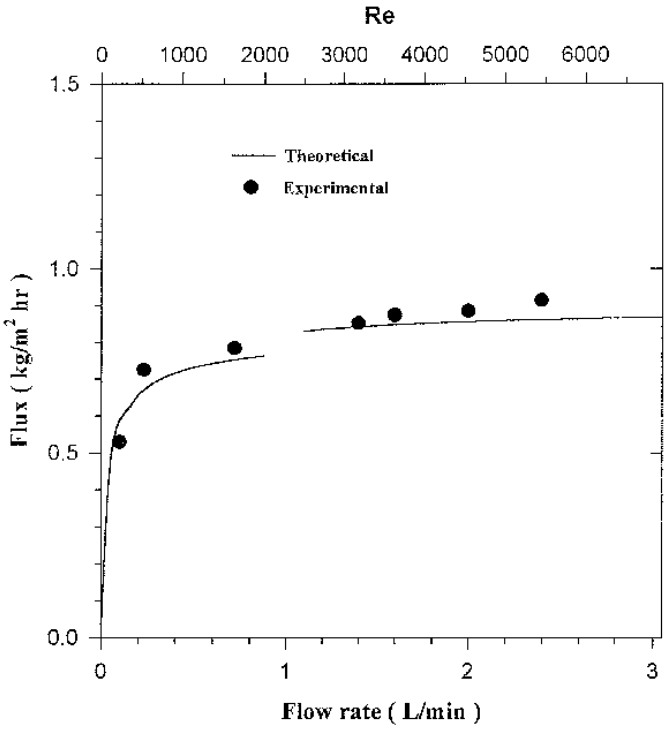

FIG. 3 Effect of saline-water flow rate on permeate flux (3 wt% NaCl, $T_h = 50°C$, $T_c = 26°C$, $\Phi_c = 1.9$ L/min).

ference across the membrane decreases. The discontinuity in Fig. 3 occurs due to the change from laminar to turbulent flow correlations. The heat and mass transfer coefficients were evaluated for these two regimes using different empirical formulas.

In Fig. 4 it is shown that cooling water flow rates have a minimal effect on the pure water flux produced. At very low flow rates the cooling water solution warms up faster, leading to a decrease in the vapor pressure difference across the membrane, and therefore a decrease in pure water flux. However, increasing the cooling water flow rate will only overcome the effect of temperature polarization. This effect will be small on the cooling side as small temperature differences at low temperatures will have a minor effect on the vapor pressure at that side.

Effect of Temperature

Figure 5 presents a comparison between model predictions and experimental results for the effect of saline water temperature on flux. The match between theoretical and experimental permeate fluxes is good. The exponential

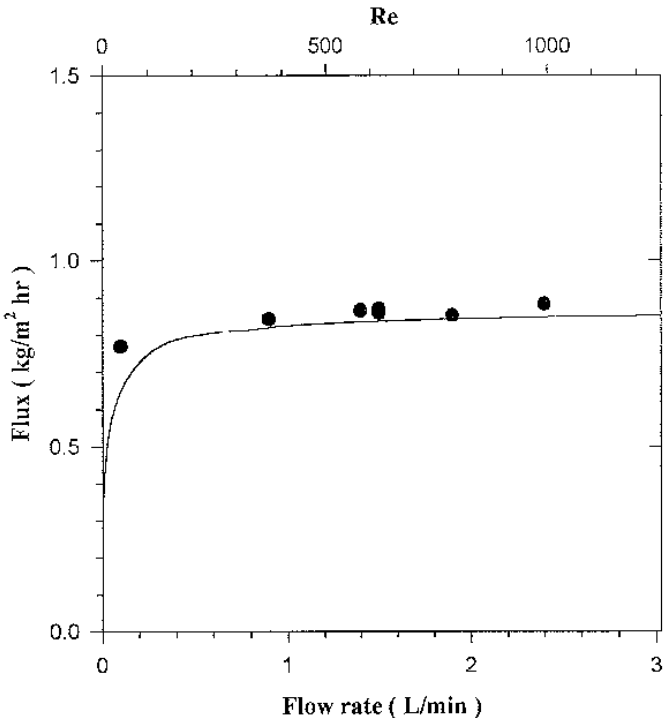

FIG. 4 Effect of cooling-water flow rate on permeate flux (3 wt% NaCl, $T_h = 50°C$, $T_c = 26°C$, $\Phi_h = 1.4$ L/min).

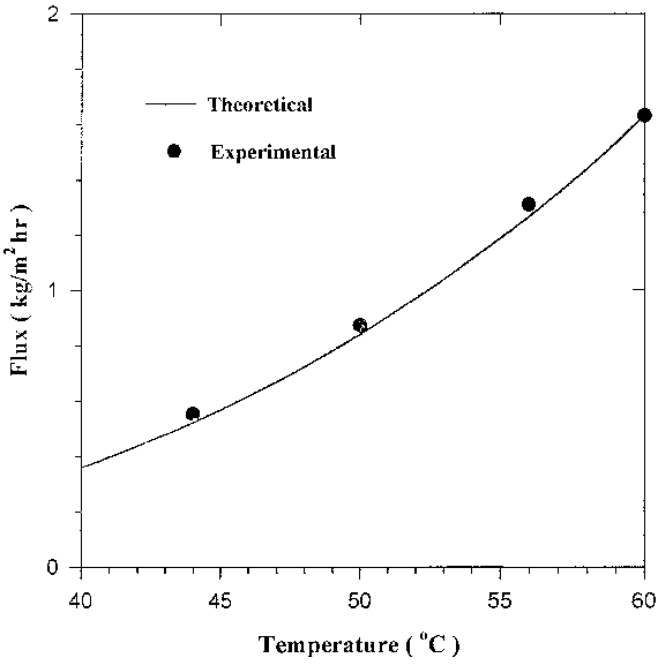

FIG. 5 Effect of saline-water temperature on permeate flux (3 wt% NaCl, $T_c = 26°C$, $\Phi_h = 1.4$ L/min, $\Phi_c = 1.9$ L/min).

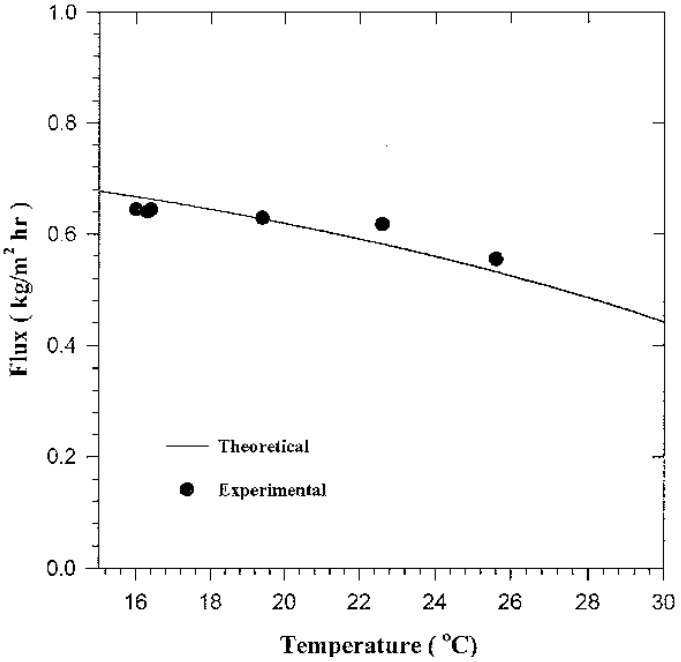

FIG. 6 Effect of cooling-water temperature on permeate flux (3 wt% NaCl, $T_h = 44°C$, $\Phi_h = 1.4$ L/min, $\Phi_c = 1.9$ L/min).

increase of permeate flux with temperature increase is attributed to the exponential dependency of water vapor pressure on temperature.

Figure 6 presents the model predictions and the experimental data for the effect of cooling water temperature on the permeate flux. Once again, there is good agreement between the model and the corresponding experimental points. Both the experimental and the theoretical permeate fluxes decrease with an increase in cooling temperature. This is because increasing the coolant temperature at a constant hot side temperature decreases the temperature difference between the hot and the cold sides and consequently reduces the vapor pressure gradient which is the driving force in this process.

The results of the present model and Lacoursiere's semiempirical model are compared to the corresponding experimental data in Fig. 7 for the effect of temperature difference on the distillate flux. As shown, both models correlate well with the experimental data; however, at a high temperature difference the developed model results follow the experimental data more closely.

Effect of Salt Concentration

Figure 8 shows the model predictions and the experimental data for the effect of feed salt concentration on the distillate flux. The model results agree well with the experimental data. The results in Fig. 8 show that as the salt con-

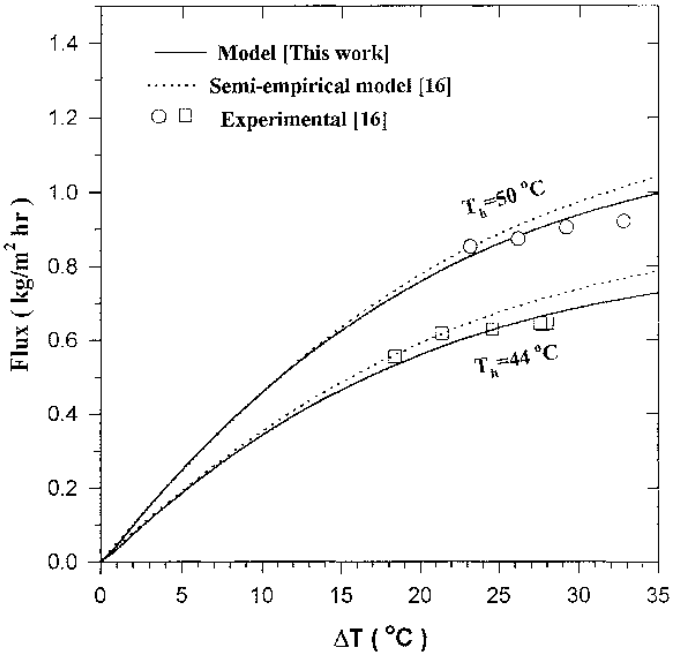

FIG. 7 Comparison of model predictions with previously published experimental and theoretical works for temperature effect on permeate flux (3 wt% NaCl, Φ_h = 1.4 L/min, Φ_c = 1.9 L/min).

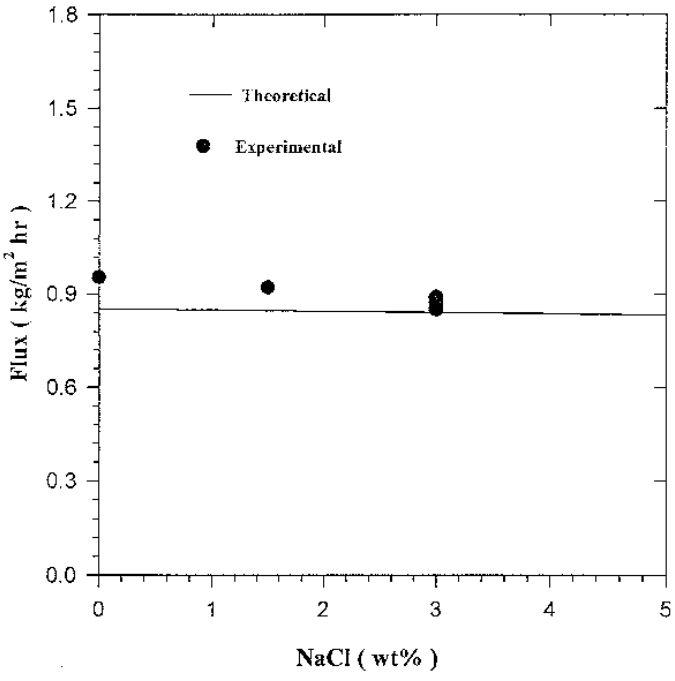

FIG. 8 Effect of feed salt concentration on permeate flux (T_h = 50°C, T_c = 26°C, Φ_h = 1.4 L/min, Φ_c = 1.9 L/min).

centration increases, the pure water flux produced decreases only slightly. This is attributed to the fact that the addition of salt reduces the partial pressure and thereby the driving force of membrane distillation.

CONCLUSIONS

An entirely predictive mathematical model was developed for desalination via tubular direct contact membrane distillation. The predicted distillate fluxes were compared to previously published experimental and theoretical data. Model predictions agreed well with the corresponding experimental data for different process variables such as saline water and coolant water flow rates and temperatures, and salt feed concentration.

NOMENCLATURE

A	surface area (m^2)
C_p	molar heat capacity (J/mol·°C)
C_t	total molar concentration (mol/m^3)
d	diameter (m)
D	diffusion coefficient (m^2/s)
F	Faraday constant (C/g-equiv)
h	heat transfer coefficient ($W/m^2 \cdot K$)
H	as specified in Eqs. (15), (22), and (25) (W/K)
k	thermal conductivity (W/m·K) or mass transfer coefficient (m/s)
l	length of membrane segment (m)
L	module length (m)
m	molar flow rate (mol/s)
n	number of tubes (—)
n^+, n^-	valences of cation and anion, respectively
$\underline{N}$	molar flux ($mol/m^2 \cdot s$)
N	molar mass transfer rate (mol/s)
Nu	Nusselt number (—)
P	total pressure (N/m^2)
$P°$	vapor pressure (N/m^2)
Pe	Peclet number (—)
Pr	Prandtl number (—)
q_s	sensible heat transfer rate (J/s)
Q	rate of heat transfer (J/s)
r	radial distance (m)
R	gas constant ($m^3 \cdot Pa/kmol \cdot K$)
Sh	Sherwood number (—)
T	temperature (K)

MARCEL DEKKER, INC.
270 Madison Avenue, New York, New York 10016

x	salt mole fraction in the liquid phase (—)
y	mole fraction of water vapor (—)

Subscripts and Superscripts

c	cooling water
d	solid
f	feed
g	gas
h	hot saline
i	internal
l	liquid
m	membrane
o	external
p	permeate
s	segment number
w	water

Greek Letters

δ	membrane thickness (m)
ε	porosity (—)
Φ	volumetric flow rate (m^3/s)
λ	latent heat of vaporization (J/mol)
λ_+°, λ_-°	limiting (zero concentration) ionic conductance (A/m^2)
μ	viscosity (kg/m·s)
ρ	molar density (mol/m^3)
τ	tortuosity factor (—)

REFERENCES

1. K. S. Spiegler, *Salt Water Purification*, 2nd ed., Plenum Press, New York, NY, 1977.
2. K. S. Spiegler and A. D. Laird, *Principles of Desalination*, 2nd ed., Academic Press, New York, NY, 1980.
3. R. Y. Huang, *Pervaporation Membrane Separation Processes*, Elsevier, Amsterdam, 1991.
4. L. Basini, G. D. Angelo, M. Gobbi, G. C. Sarti, and C. Gostoli, *Desalination*, *64*, 245 (1987).
5. D. W. Gore, "Gore-Tex Membrane Distillation," in *Proceedings of the 10th Annual Convention of the Water Supply Improvement Association*, *Honolulu*, *Vol. III*, 1982, p. 1.
6. S. I. Andersson, N. Kjellander, and B. Rodesjo, *Desalination*, *56*, 345 (1985).
7. R. W. Schofield, A. G. Fane, and C. J. Fell, "Membrane Distillation—A Novel Evaporation Process," in *Proceedings of the 13th Australian Chemical Engineering Catalyst 'Chemeca 85,' Perth*, 1985, p. 295.
8. E. Drioli and W. Yonglie, *Desalination*, *53*, 339 (1985).
9. A. G. Chmielewski and G. Zakrzewska-Trznadel, *Sep. Sci. Technol.*, *30*, 1653 (1995).

10. F. Banat and J. Simandl, *Desalination, 95*, 39 (1995).
11. G. C. Sarti, C. Gostoli, and S. Matulli, *Ibid*., *56*, 277 (1985).
12. S. Kimura and S. Nakao, *J. Membr. Sci*., *33*, 285 (1987).
13. F. Banat and J. Simandl, *Sep. Sci. Technol*., *33*, 201 (1998).
14. R. W. Schofield, A. G. Fane, C. J. Fell, and R. Macoun, *Desalination, 77*, 279 (1990).
15. R. W. Schofield, A. G. Fane, and C. J. Fell, *J. Membr. Sci*., *53*, 159 (1990).
16. A. G. Fane, R. W. Schofield, and C. J. Fell, *Desalination, 64*, 231 (1987).
17. S. Lacoursiere, "Water Purification by Membrane Distillation," M.Eng., McGill University, Canada, 1994.
18. L. Martienz-Diez and M. I. Vazques-Gonzalez, *AIChE J*., *42*, 1844 (1996).
19. C. Geankoplis, *Transport Processes and Unit Operations*, 3rd ed., Prentice-Hall, Englewood Cliffs, NJ, 1993.
20. R. C. Reid, J. M. Prausnitz, and B. E. Poling, *The Properties of Gases and Liquids*, 4th ed., McGraw-Hill, New York, NY, 1987.
21. J. R. Welty, C. E. Wicks, and R. E. Wilson, *Fundamentals of Momentum, Heat, and Mass Transfer*, 3rd ed., Wiley, New York, NY, 1984.

Received by editor March 26, 1998
Revision received October 1998

Request Permission or Order Reprints Instantly!